CILAMCE 2016

XXXVII IBERIAN LATIN AMERICAN CONGRESS ON COMPUTATIONAL METHODS IN ENGINEERING
BRASÍLIA - DF - BRAZIL

NUMERICAL ANALYSIS OF THE IN-CYLINDER FLOW FIELD AND COMPARISON WITH EXPERIMENTAL DATA IN A SINGLE CYLINDER RESEARCH ENGINE

Raphael Meireles Braga

Leonardo Mayer Reis

Leonardo Guimarães Fonseca

Rudolf Huebner

Ramon Molina Valle

raphaelmeirelesb@gmail.com

leo1mayer@gmail.com

leo1fonseca@gmail.com

rudolf@demec.ufmg.br

ramon@demec.ufmg.br

Federal University of Minas Gerais

Pres. Antônio Carlos Avenue, 6627, 31270-901, Minas Gerais, Belo Horizonte, Brazil

Abstract. *In this paper, the 3D numerical analysis of the flow field in a single cylinder research engine with optical access, running cold flow, is presented. The simulations were carried out in the commercial software Star-CD with es-ICE module and the two different turbulence models: RNG-k-ε and k-w SST were compared with experimental data of the engine running at 1000 rpm in motored conditions. A grid independency study is presented using five grids varying from approximately 500,000 to 1,500,000 cells on piston bottom dead center. An optical window inside the engine cylinder was used to measure the velocity components along the crank angle with the PIV technique and a comparison was made with calculated velocity curves. Moreover, a qualitative analysis of the scalar flow field in the region of interest is presented. The results showed a better agreement with the RNG-k-ε and experimental mean velocity magnitude curve than k-ω-SST. However, the qualitative scalar velocity field of the k-ω model captured more details of the flow than the k-ε model.*

Keywords: Turbulence, Internal Combustion Engine, Star-CD, 3D Simulation, RANS

1   INTRODUCTION

Currently, with the air pollution issue and nonrenewable energy sources highlighted in combination with increasing restrict emissions standards, replacements for internal combustion engines (ICE) are been researched, for instance the electric engine and the hydrogen fuel cells. On the other hand, automotive fleet moved by ICE is increasing more and more with time. According to National Association of Automotive Vehicle Manufactures (ANFAVEA), near 3.7 million vehicles have been produced in Brazil in 2013. This suggests that ICEs will be vehicle main power system for following decades until the next generation of power systems takes its place. Given that, it is crucial that vehicles manufactures continue developing new technologies to improve engines overall performance, reduce specific fuel consumption and as a consequence, reduce greenhouse gas emissions.

The in-cylinder air flow is directly related to power, fuel consumption and pollutant emission as it is responsibly to enhance the flame propagation and the air fuel mixture formation (Li et al., 2001). It is also important to highlight that an optimum value for flow intensity exists, given that too much of that can disturb the kernel formation or lead to excessive wall heat transfer, which can reduce torque, power and increase hydrocarbon emissions (Hill e Zhang et al., 1994; Aita et al., 2005; Li et al., 2001). The in-cylinder large scale air motion can be classified basically into two: tumble and swirl. The first one is the loop movement and the second is the rotation around cylinder axis and both take place simultaneous during engine operation. They can be evaluated using the tumble ratio and swirl ratio, which are dimensionless numbers that compare the angular velocity of the flow with the angular velocity of the crankshaft (Lumley, 1999) - Equation 1 shows the tumble and swirl ratios, where ω_s and ω_t are the angular velocities of the swirl and tumble motion and ω_e is the crankshaft angular velocity.

$$R_s = \frac{\omega_s}{\omega_e} \qquad R_t = \frac{\omega_t}{\omega_e} \tag{1}$$

The angular velocity of the flow can be calculated using the vorticity ($\vec{\zeta}$) vector:

$$\vec{\zeta} = 2\vec{\omega} = \left(\frac{\partial w}{\partial y} - \frac{\partial v}{\partial z}\right)\hat{\imath} + \left(\frac{\partial u}{\partial z} - \frac{\partial w}{\partial x}\right)\hat{\jmath} + \left(\frac{\partial v}{\partial x} - \frac{\partial u}{\partial y}\right)\hat{k} \tag{2}$$

Thus, the tumble and swirl coefficients are given by Equation 3:

$$R_s = \frac{\frac{\partial u}{\partial z} - \frac{\partial w}{\partial x}}{2\omega_e} \qquad R_t = \frac{\frac{\partial w}{\partial y} - \frac{\partial v}{\partial z}}{2\omega_e} \tag{3}$$

There are many ways to visualize and measure the in-cylinder flow. First of all, is by experimental methods, which has been widely investigated using Laser Doppler Anemometry, LDA (Le Coz et al., 1990; Fansler 1988, Lee 2000) and using Particle Image Velocimetry, PIV (Rouland et al., 1997; Marc 1997, Choi et al., 1999; Reuss 2000, Li et al., 2001). Experimental setups however, are not simple due to engine cycle to cycle variation even

under best experimental conditions (Hill and Zhang, (1994); Chen et al., 1998) and also they are costly (Kurniawan et al., 2007).

Another option to study the engine air flow is using Computational Fluid Dynamics (CFD). This technique combined with experimental results can provide very reliable data and help on detecting engine abnormal behavior, what can substantially reduce prototyping phase time. CFD technique bases on solving continuity, momentum, energy and also turbulence equations (more details can be found in Versteeg & Malalasekera, 2009). Although CFD has become a strong ally on research and development of internal combustion engines, the simulations requires experimental data as boundary conditions as well as for validation. Among several turbulence models that are based on Reynolds-averaged Navier-Stokes equations (RANS) the more commonly validated and used is the k-ε family (Versteeg & Malalasekera, 2009). The k-ε RNG (re-normalization group) was developed by Yakhot et al. (1992) and when compared with the standard k-ε model have an additional term on the dissipation equation that takes into account the effects of the mean flow distortions on the turbulence. Another interesting turbulence model is the Menter SST k-ω which was developed in 1993 and is a combination of the k-ε model on free flow region and the k-ω on the near wall region. Their equations will not be described in this paper for sake of brevity, but can be found in Yakhot et al. (1992) and Menter (1994).

In the numerical field, Chen et al. (1998) simulated a diesel engine, two valves with transparent liner and investigated the port and in-cylinder flow for 1000 and 2000 rpm using the k-ε standard and compared with LDA measurements. The author claimed that this turbulence model is unable to accurately simulate the effects of streamwise pressure gradients in the flow. Payri et al. (2003) studied a diesel 4 valves engine for different combustion chambers using the RNG k-ε and compared the results with LDV measurements. The maximum differences between experimental and numerical results are again associated with the lack of accuracy of the k-ε model in the presence of strong swirl motion. Toh et al. (2011) utilized Star-CD software and standard k-ε model to analyze two different intake port flow configurations: one with an elliptical cross section area and another with a circular one. The results have shown that the one with the elliptical port is more susceptible to tumble formation. Qi et al. (2012) simulated a single cylinder spark ignition engine using KIVA and Star-CD software to optimize the intake port. The results showed that by increasing tumble coefficient, the fuel vaporization increased 20%, which reduced hydrocarbons emissions especially when the fuel injection happed with a cold engine.

The aim of this paper is the 3D simulation of the in-cylinder flow field of a single cylinder spark ignition engine. Two different RANS turbulence models were used and comparisons of the velocity data and scalar field between the simulation PIV measurements were made.

2   METHODOLOGY

2.1   Computational domain

The engine studied in this work is a single cylinder research engine (SCRE) with a quartz liner, which allows the visualization of multiple phenomena inside the cylinder. The engine is a four valve spark ignition with a flat piston and its main characteristics are shown in Table 1.

Table 1. Main engine characteristics

Item	Dimensions
Bore	82 mm
Stroke	86 mm
Displaced volume	454.2 cm³
Compression ratio	9.3:1
Connecting rod length	144 mm
Intake valve diameter	31.1 mm
Exhaust valve diameter	28.0 mm
Maximum intake lift	10.49 mm
Maximum exhaust valve lift	9.51 mm
Intake valve open at	5º BTDC @ 0.25 mm
Intake valve close at	210º ATDC @ 0.25 mm
Exhaust valve open at	230º BTDC @ 0.25 mm
Exhaust valve close at	10º ATDC @ 0.25 mm

The internal volume of the engine head (combustion chamber and ports) and the manifolds were extracted and used as computational domain. To reduce computational costs, the symmetry condition was used in the grid independency study. Figure 1 a) is a scheme showing the symmetry condition of the engine and Figure 1 b) shows the computational domain.
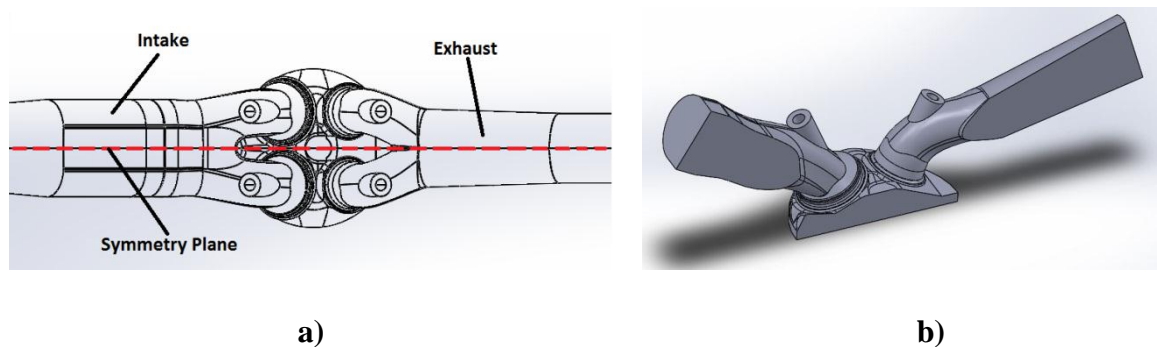

a)   b)

Figure 1. Symmetry plane: a); computational domain: b)

2.2   Mesh Generation

The grid generation was made using the es-ICE module and the trimmed method, in which a base template is used to make several meshes during the engine cycle through addition and removal of cell layers, in order to represent the movements of valves and piston. The manifolds mesh was made using Star-CCM+ and thereafter attached to the engine head mesh. Figure 2 shows the base head and cylinder mesh used on the simulations and Figure 3 shows the coupling between this mesh and the manifolds mesh.
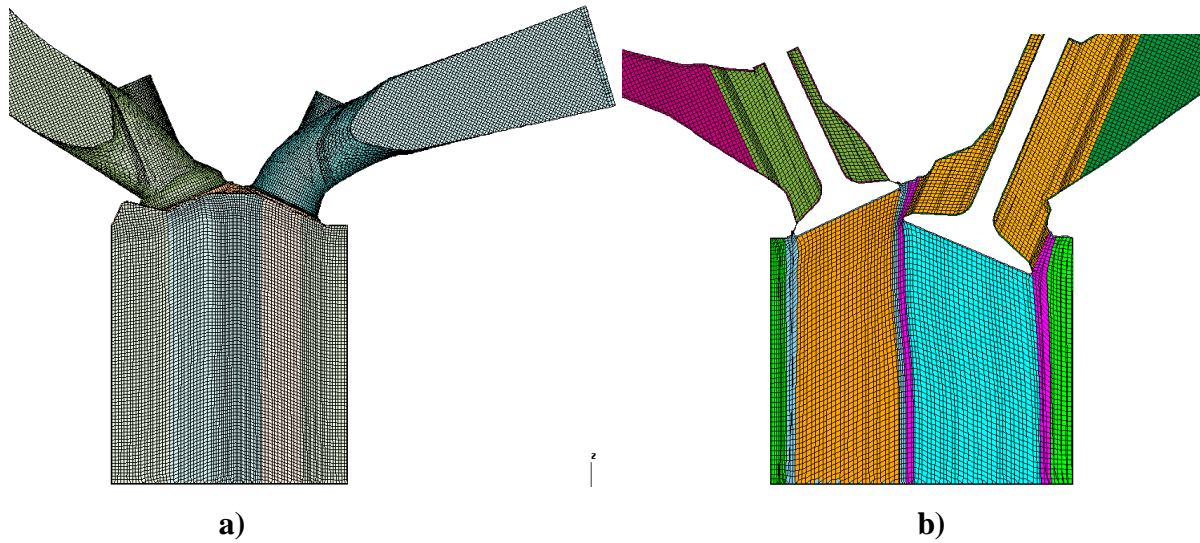
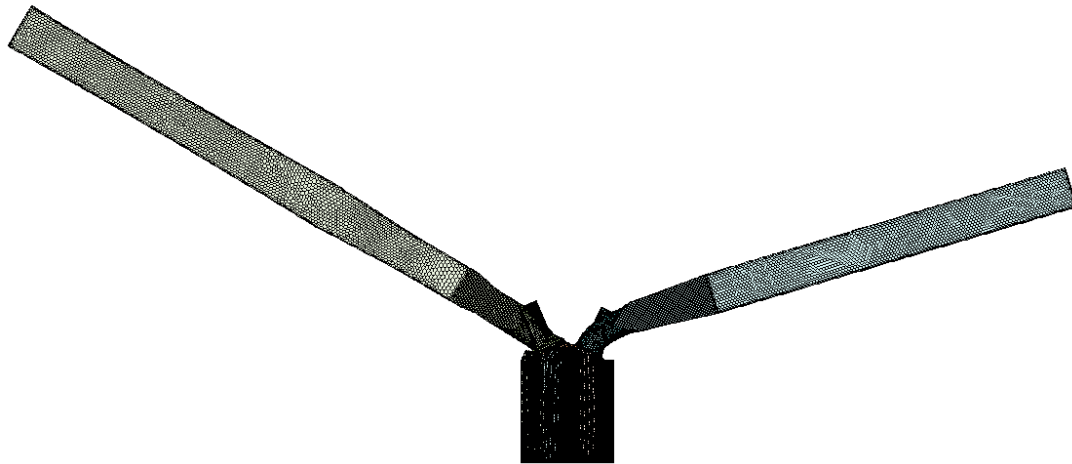**Figure 2. Grid used in the simulations: a); cross sectional view of the grid: b)**

Figure 3. Coupling the manifolds mesh

2.3   Boundary and Initial Conditions

The boundary conditions were obtained with the engine operating at 1000 rpm and wide open throttle under motoring conditions, in which the dynamometer is used as an electric motor in order to provide the required power. Pressure as a function of the crank angle was measured at intake and exhaust manifold (Figure 4) and also the mean air temperature of that boundaries were measured and set equal to 301 K and 304 K respectively. As initial conditions, pressure and temperature as a function of crank angle in the cylinder region were used (Figure 5) and also the same pressure plot used as boundary conditions for the intake and exhaust regions were used as initial conditions of those regions. The combustion dome, cylinder wall and piston temperatures were set as 333 K and the intake and exhaust manifolds as well as the valves were considered adiabatic.
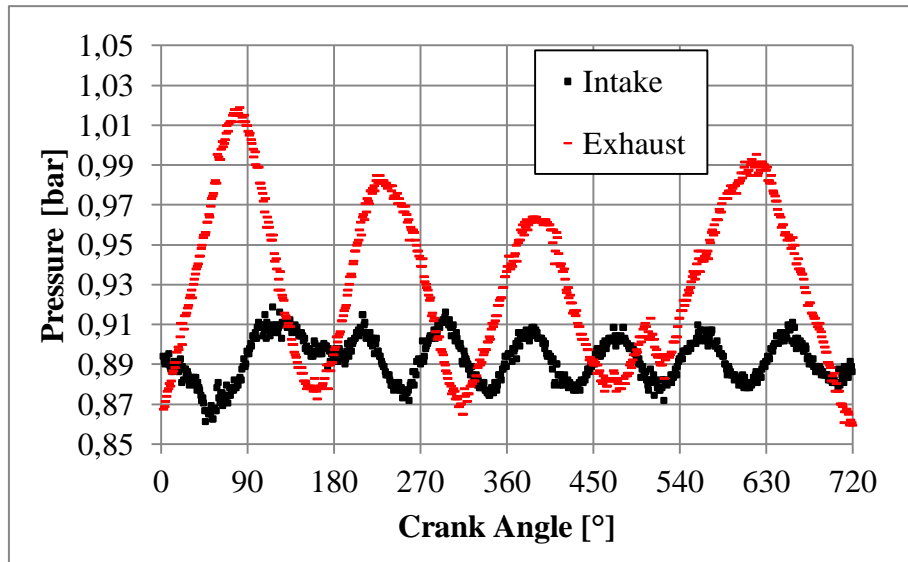
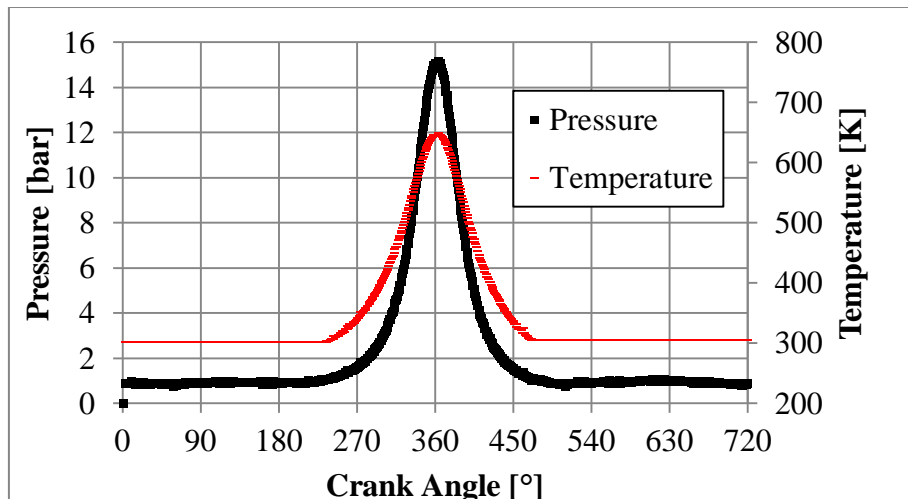**Figure 4. Pressure curves used as boundary conditions for the intake and exhaust regions**

Figure 5. Pressure and temperature curves used as initial condition for the cylinder region

2.4   Simulations Parameters

To increase the reliability of the results, three cycles of the engine were simulated and the third one was used for the analysis. The engine speed was 1000 rpm and the time step was 0.05 crank angle degrees ($8x10^{-7}$ s). The residual tolerances were set equal to 10^{-4} for pressure, momentum and temperature equations and 10^{-3} for turbulence equations. Only air was induced into the engine and no combustion took place (cold flow analysis) and the simulations were carried out on the Star-CD software. Two turbulence models were used: the RNG k-ε and the k-ω SST.

CILAMCE 2016

Proceedings of the XXXVII Iberian Latin-American Congress on Computational Methods in Engineering
Suzana Moreira Ávila (Editor), ABMEC, Brasília, DF, Brazil, November 6-9, 2016

2.5   Grid Independency Study

A grid independency study was carried out using five grids and the refinement factor was a raise of 1.3 times the number of cells on the bottom dead center of the previous grid starting from a base grid of 500,000 cells. Table 2 shows the total number of each grid. Due to computational limitations, this study was made only for the RNG k-ε model and the symmetry condition was used.

Table 2. Grids of the grid independency study

Grid	N_{total}
G1	488,787
G2	660,377
G3	836,655
G4	1,179,349
G5	1,500,165

As a convergence criterion, the average velocity magnitude in three planes was used: one was the symmetry plane, another one was orthogonal of the symmetry plane and passing between the valves and the last one is orthogonal of z axis and placed 3 mm below the cylinder head. It was established that a grid would be considered satisfactory provided that a pair of consecutives grids present differences smaller than 5%. Since it is a transient analysis, this criterion should be achieved in at least 90% of the analyzed points during the intake and compression strokes of the engine. To illustrate the results of this study, Figure 6 shows the average velocity magnitude on the plane between the valves for the five grids. Following that criterion, the Grid G4, with proximately 1,800,000 cells on bottom dead center, was considered acceptable and used for further analysis. By using the grid G4 it took 34 hours to run one cycle of the engine using 32 processors workstation. After the selection of the grid, to run the final cases, the complete domain was used (no symmetry condition) and the complete mesh was just a duplication of the previous one.
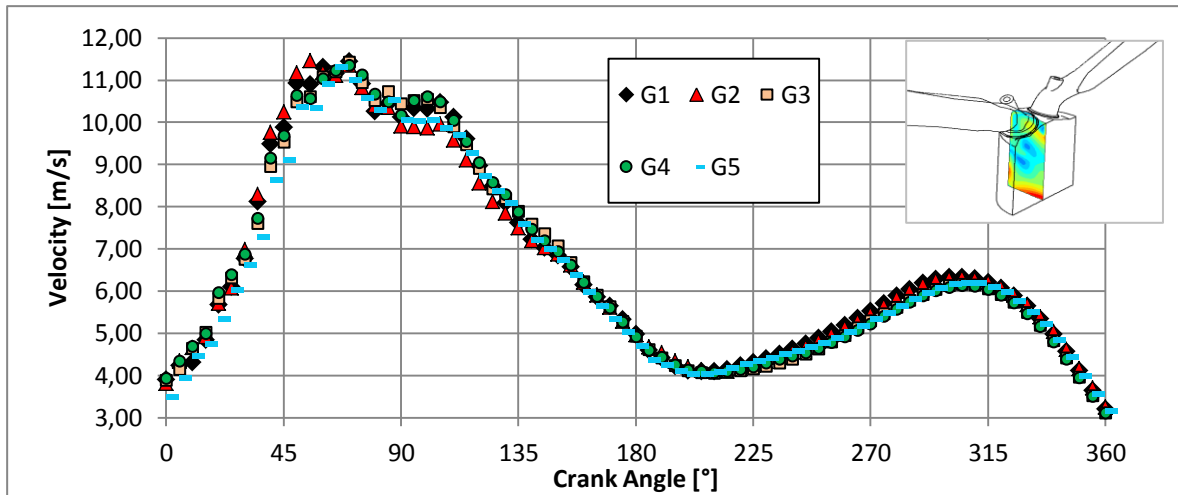
Figure 6. Average velocity magnitude of the x axis perpendicular plane for the five grids used on the grid independency study

2.6 Experimental Setup

The experimental setup was made with the engine running at 1000 rpm and wide open throttle. The PIV used was Litron LDY302 PIV with a frequency of 1 kHz and vegetable oil was inoculated as the particles. A high speed camera Phantom v9.1 was used to capture the successive images of the dispersed phase. The measurements were made in the symmetry plane of the engine (Figure 7 a) and the images were taken at a lateral visualization window of 36 mm width and 40 mm height shown at Figure 7 b) This windows allows complete visualization between approximately 90º crank angle and approximately 260º crank angle of the intake and compression strokes, out of this range the window is partially or completely obstructed by the piston motion. Ten cycles were run and the data obtained was treated using Dantec Dynamics – Dynamic Studio 3.41.38. More details of the experimental methodology can be obtained at Gomes (2015).
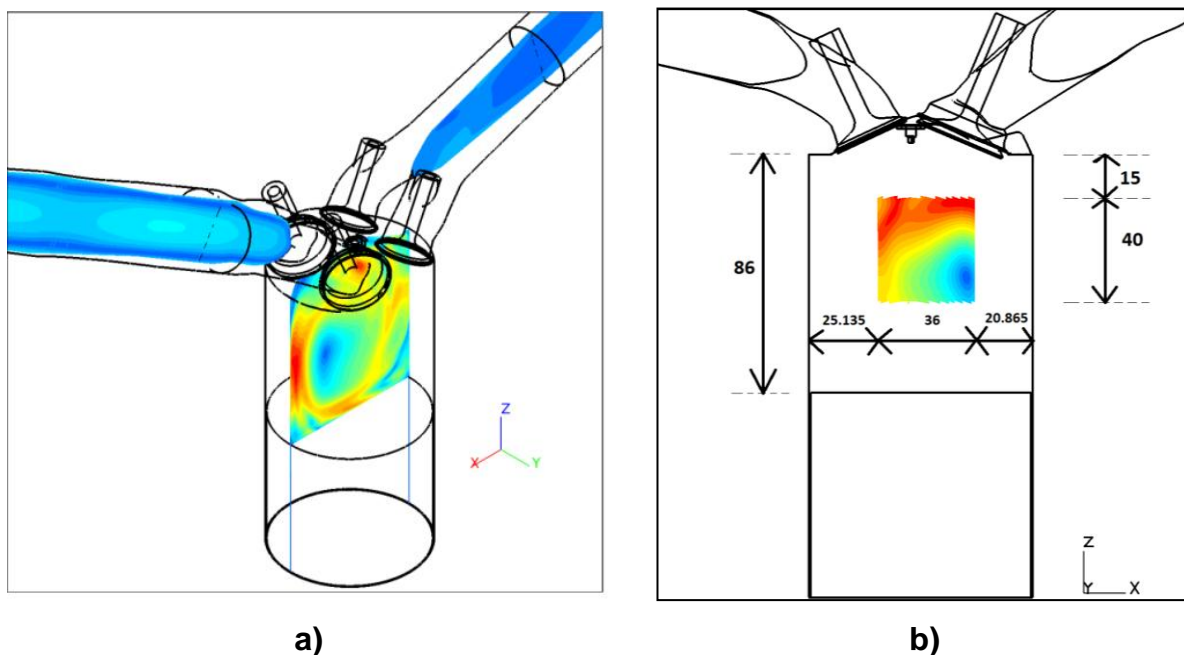

a)   b)

Figure 7. Optical window plane: a); measurements window dimensions: b)

3   RESULTS

Pressure is a variable that is not strongly dependent of the turbulence model and the In-cylinder pressure varied less than 0.5% between the two turbulence models. Since the pressure plot is almost the same in both simulations, only RNG k-ε is compared with experimental in-cylinder pressure (Figure 8). The maximum difference between numerical and experimental pressure happens on the pressure peak and its magnitude is 6%.
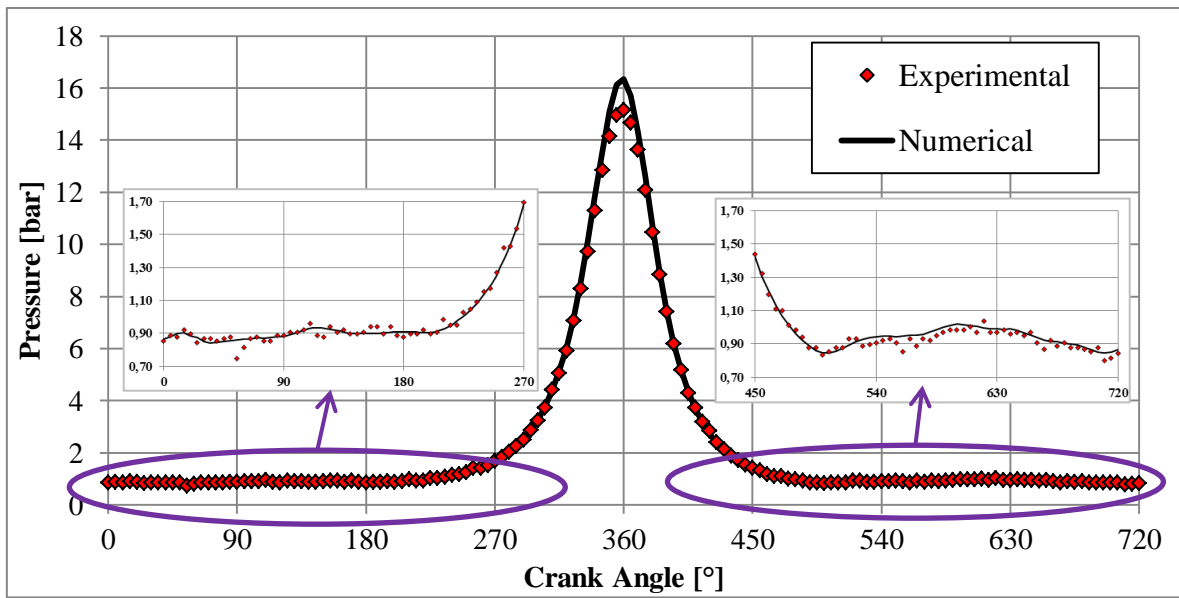

Figure 8. In-cylinder pressure plot

The k-ε model took approximately 106 hours per cycle while the k-ω model was slightly more costly and took 117 hours per cycle. The U velocity (in x axis direction) and W (in z axis direction) in the window region were extracted both numerically and experimentally and the velocity magnitude of them were compared. Figure 9 shows the average velocity magnitude as a function of crank angle during the intake and compression stroke for the simulations using the RNG k-ε, k-w SST as well as for experimental case. Based on Figure 9 is possible to see that in both turbulence models the velocity curve has the same general behavior as the experimental curve. However, some differences can be seen, especially at the beginning and at the end of the curve. The phase and magnitude of the velocity peak is not well predicted in both models. In addition, the numerical curves present an earlier velocity valley than the experimental one. The RNG k-ε model has shown very good results during the crank angle interval between 135º and 180º.

The average tumble ratio was calculated using the vorticity approach on each cell in the window region and Figure 10 shows its values as function of crank angle for numerical and experimental cases. Both turbulence models over predicted the tumble ratio, however, they showed the same tendency as the experimental data, for instance they showed a maximum value near 100 CAD (crank angle degree) and a minimum value near 135 CAD. Based on Figure 10 it is possible to point out that the flow has the same rotational direction during the entire analysis interval.
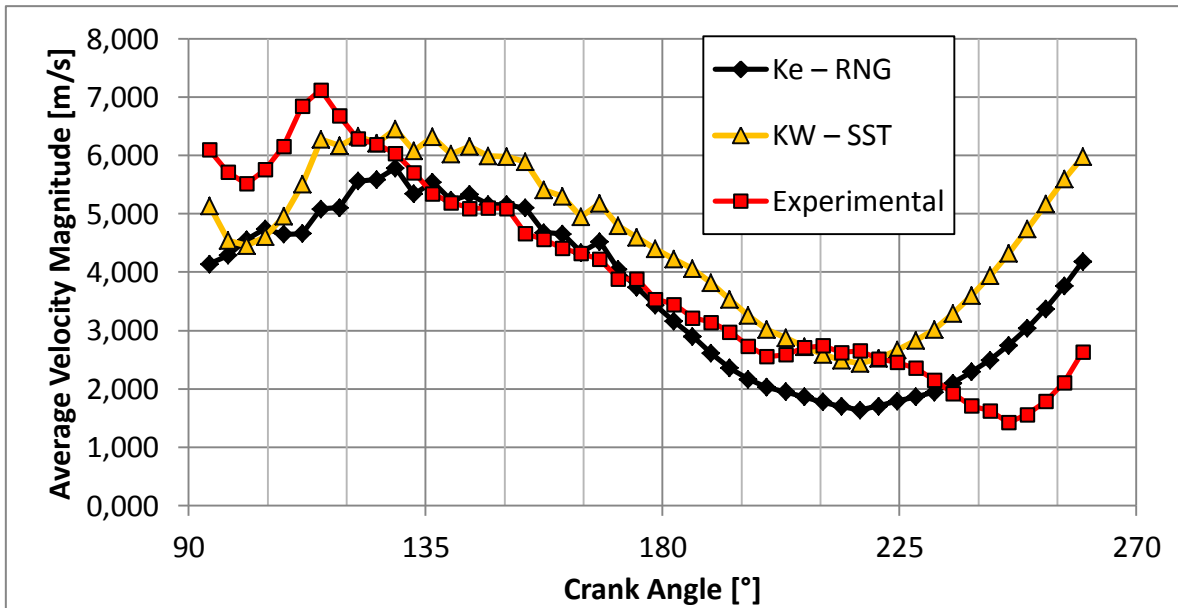
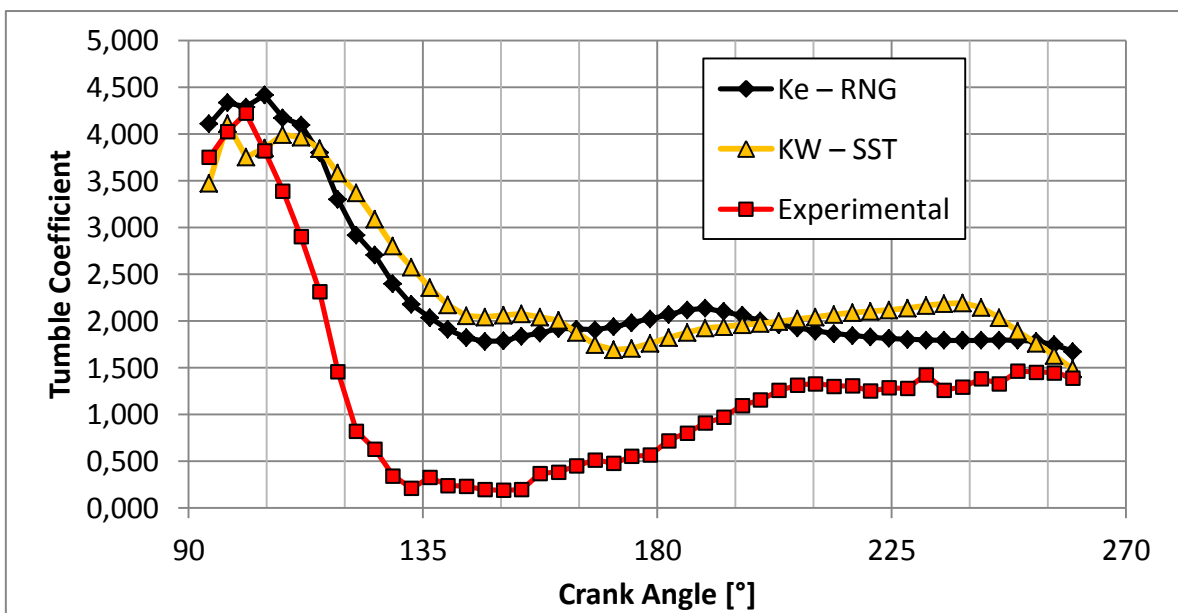**Figure 9. Average Velocity Magnitude in the window region for the RNG k-ε, k-ω SST and experimental data**

Figure 10. Tumble coefficient for RNG k-ε, k-ω SST and experimental cases

Based on the velocity magnitude plot of the Figure 9 three crank angle degrees were chosen to analyze the scalar flow field: the velocity peak (115º), the bottom dead center (180º) and the point where the greatest absolute differences took place (260º). The calculated and measured scalar velocity fields at these three crank angles are shown at Figure 11.
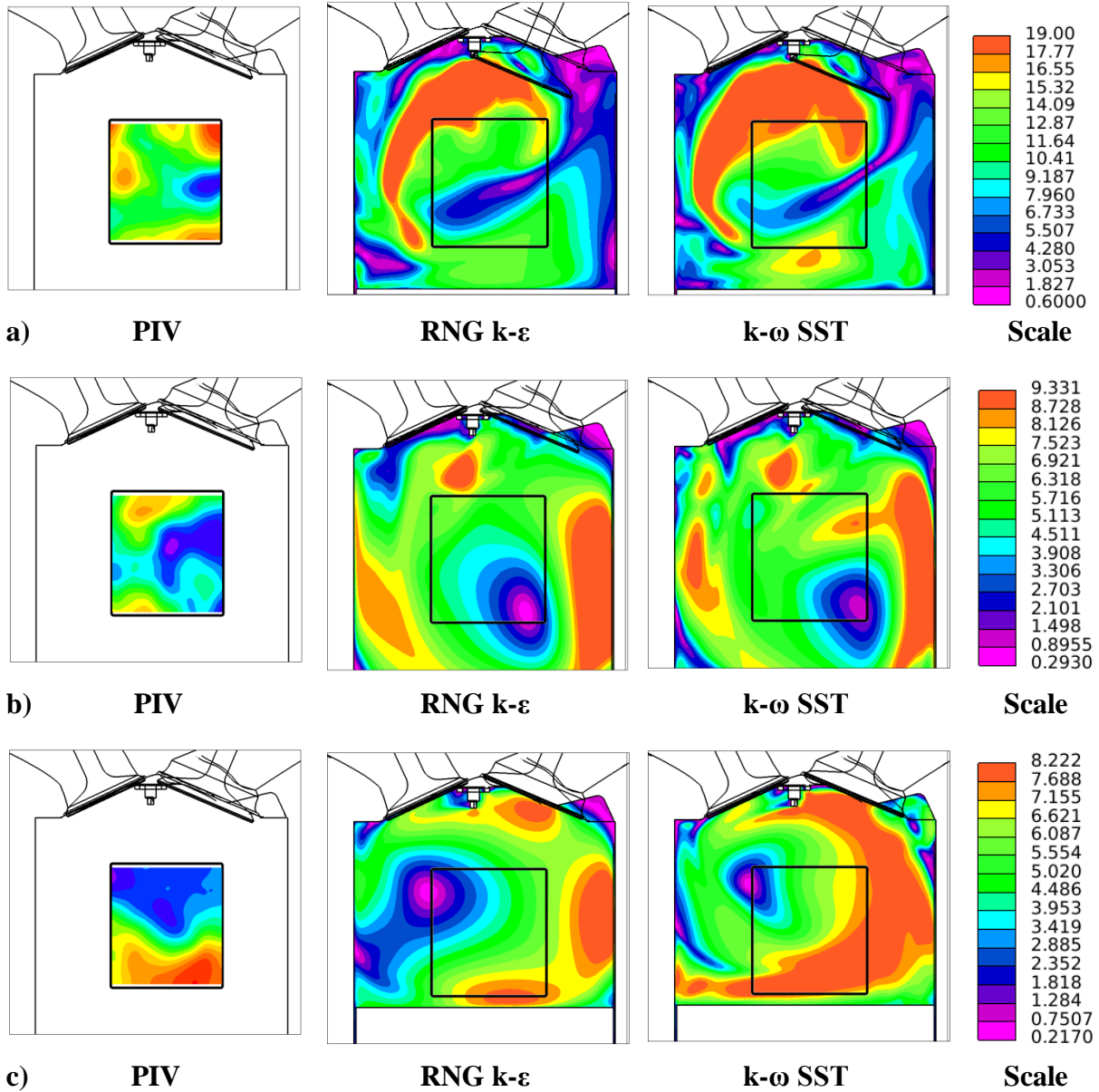
Figure 11. Velocity magnitude scalar field for the PIV measurements, RNG k-ε and k-ω SST at 115º: a) 180º: b) e 260º: c)
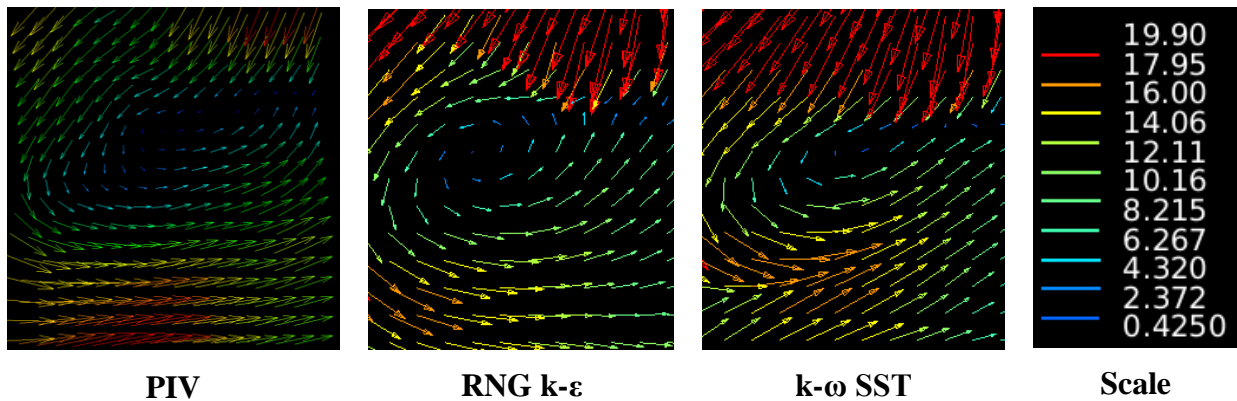

Figure 12. Velocity vector field

Based on Figure 11 a, it is possible to realize that the models present the same flow pattern: one jet with high velocities on the top of the image, a central vortex amid of the cylinder with counter clockwise (Figure 12) and some secondary vortex near the cylinder head and cylinder wall. The k-ω model presented a larger area with higher velocities and a smaller central vortex area than the RNG k-ε model. Comparing with the experimental data, despite both models over predicted the length of the central vortex, they presented the same flow structure: one region with high velocities on the top of the analysis window, one region with low velocities on the center of the window. Especially on the k-ω model it is possible to see a region of high velocities on the bottom of the window just as the experimental case.

On the Figure 11 b all images show a low velocity region on the right side of the analysis window. Both models present a high velocity region on the right side of the cylinder, but on the k-ω model this region enters the window area like on the PIV image. On the last crank angle (Figure 11 c) a region with low velocity is found on the upper left side of the window and on the three cases a vortex can be seen. Both models calculated a high velocity region on the right side of the cylinder; on the k-ε model this region is divided in three: one on the bottom, other on the right and another one on the top of the cylinder. On the k-ω model this regions are connected and present more details than the RNG k-ε. Moreover, on the upper right corner of the cylinder on the k-ω SST model case is possible to see a well-defined vortex, while on the RNG k-ε there is just a region with low velocities. Comparing with the PIV image, both models show agreement predicting higher velocities on the bottom right side and with a vortex on the upper left side of the window. However, on the PIV image this region with lower velocity is larger than the models predicted.

4 CONCLUSIONS

To summarize, the calculated in-cylinder pressure curve showed a reasonable agreement with the experimental curve along the cycle, but on the pressure peak a difference of 6% was seen. Both turbulence models presented the same velocity curve tendency of the experimental, but they were not able to satisfactory predict the velocity peak and valley. In addition, both models over-predicted the tumble ratio on the window region, but again they could capture the curve tendency. The scalar velocity field showed that the turbulence models could give a general idea of the main in-cylinder flow pattern, but some significant magnitude differences were seen when compared to the PIV image which is related to the deficiency of the models as well as the fact that only few cycles were used to build the experimental data which might not be sufficient to have a mean flow like the one given on the simulations.

5   *Acknowledgements*

REFERENCES

Aita, S.; Tabbal, A.; Munck, G.; Montmayeur, N.; Takenaka, Y.; Aoyagi, Y.; Obana, S. Numerical simulation of swirling port-valve-cylinder flow in diesel engines, *SAE technical paper* N. 910263, Warrandale, 1991.

Chen, A.; Veshagh, A.; Wallace, S. Intake predictions of a transparent DI diesel engine. *SAE technical paper* N. 981020, Warrandale, 1998.

Choi, K. H.; Park, J. H.; Lee, N. H.; Yu, C. H.; Noh, S. H., A research on fuel spray and air fields for spark-ignited direct injection using laser measurement technology. *SAE technical paper* N. 1999-01-0503, Warrandale, 1999.

Fansler, T. D.; French, D. T. Cycle-resolved laser-velocimetry measurements in a reentrant-bowl-in-piston engine. *SAE technical paper* N 880377, 1988.

Gomes, C., da Costa, R., Franco, R., Valle, R. et al., "PIV Measurements of In-Cylinder Tumble Flow in a Motored Single Cylinder Optical Research Engine," *SAE Technical Paper* 2015-36-0305, 2015.

Hill, P. G.; Zhang, D.The effect of swirl and tumble on combustion in spark ignition engines, Prog. *Energy Combust. Sci.*, 20:373-429, 1994.

Kurniawan, W. H.; Abdullah, S.; Shamsudeen, A.A computational fluid dynamics study of cold-flow analysis for mixture preparation in a motored four-stroke direct injection engine.*Journal of applied sciences* 7 (19), pp. 2007-2724, 2007.

Lee, K. C., Hill, N. S., Asadamongkon, P., & Strand, L. W. A study of turbulence and cyclic variation levels in internal combustion engine cylinders. *Proceedings of the 10th International Symposium on Applications of Laser Techniques to Fluid Mechanics*, Paper. Vol. 22., 2000.

Le Coz, J. F.; Henriot, S.; Pinchon, P.An experimental and computational analysis of the flow field in a four-valve spark engine – focus on cycle-resolved turbulence. *SAE technical paper* N. 900056, Warrandale, 1990.

Li, Y.; Zhao, H.; Peng, Z.; Ladommatos, N. Analysis of tumble and swirl motions in a four valve si engine. *SAE technical paper* N. 2001-01-3555, Warrandale, 2001.

Lumley, J. L. Engines – an introduction. *Cambridge Univesity Press*, 1999.

Marc, Daniel, et al. Tumbling vortex flow in a model square piston compression machine: PIV and LDV measurements. No. 972834. *SAE Technical Paper*, 1997.

Menter, F. R. (1994), "Two-Equation Eddy-Viscosity Turbulence Models for Engineering Applications", *AIAA Journal*, vol. 32, no 8. pp. 1598-1605.

Payri, F.; Benajes, J.; Margot, X.; Gil, A. CFD modeling of the in-cylinder flow in direct injetion diesel engines.Elsevier: *Computer &Fluids* 33 (2004) 995-1021. doi:10.1016/j.compfluid.2003.09.003.

ANFAVEA, "Produção, vendas e exportação de autoveículos. Associação Nacional dos Fabricantes de Veículos Automotores", Associação Nacional dos Fabricantes de Veículos Automotores (ANFAVEA). Available at *http://www.anfavea.com.br/*. Access in Oct. 2014.

Qi, Y.L.; Dong, L.C.; Liu, H.; Puzinauskas, P.V. And Midkiff, K.C. Optimization of intake port design for SI engine.*International Journal of Automotive Technology*, Vol. 13, No. 6, p. 861-872, 2012.

Reuss, D. L., and M. Rosalik. PIV measurements during combustion in a reciprocating internal combustion engine. *Laser Techniques Applied to Fluid Mechanics*. Springer Berlin Heidelberg, 2000. 441-456.

Rouland, E.; Trinite, M.; Dionnet, F.; Floch, A.; Ahmed, A. Particle image velocimetry measurements in a high tumble engine for in-cylinder flow structure analysis. *SAE technical paper* N. 972831, Warrandale, 1997.

Toh H.; Huang, R.; Lin, K. E Chern, M.J. Computational Study on the Effect of Inlet Port Configuration on In-Cylinder Flow of a Motored Four-Valve Internal Combustion Engine. *Journal of Energy Engineering*, Vol. 137, pp. 198-206, 2011.

Versteeg H. K., Malalasek-εra W. "An introduction to computational fluid Dynamics". 2ª ed. Pearson Prentice-Hall. 2009. 517p.

Yakhot, V., Orszag, S.A., Thangam, S., Gatski, T.B. & Speziale, C.G. (1992), "Development of turbulence models for shear flows by a double expansion technique", *Physics of Fluids A*, Vol. 4, No. 7, pp1510-1520.